

Investigation of the $^{23}\text{Na}(p, \gamma)^{24}\text{Mg}$ and $^{23}\text{Na}(p, \alpha)^{20}\text{Ne}$ reactions via $(^3\text{He}, d)$ spectroscopy

S. E. Hale,¹ A. E. Champagne,¹ C. Iliadis,¹ V. Y. Hansper,¹ D. C. Powell,¹ and J. C. Blackmon²

¹*University of North Carolina at Chapel Hill, Chapel Hill, North Carolina 27599-3255, USA
and Triangle Universities Nuclear Laboratory, Durham, North Carolina 27708-0308, USA*

²*Physics Division, Oak Ridge National Laboratory, Oak Ridge, Tennessee 37831, USA*

(Received 18 December 2003; published 7 October 2004)

States near the $^{23}\text{Na}+p$ threshold in ^{24}Mg were investigated using the $^{23}\text{Na}(^3\text{He}, d)^{24}\text{Mg}$ reaction over the angular range of $5^\circ \leq \theta_{\text{lab}} \leq 35^\circ$ at $E(^3\text{He})=20$ MeV. Spectroscopic factors were extracted for states corresponding to resonances in the $^{23}\text{Na}(p, \gamma)^{24}\text{Mg}$ and $^{23}\text{Na}(p, \alpha)^{20}\text{Ne}$ reactions. We find that one state, corresponding to a previously unobserved resonance at $E_{\text{c.m.}}=138$ keV, may make a significant contribution to the rates of both reactions at low temperatures. Another state, corresponding to a possible resonance at $E_{\text{c.m.}}=37$ keV may make a small contribution to the $^{23}\text{Na}(p, \alpha)^{20}\text{Ne}$ reaction. New rates for the $^{23}\text{Na}(p, \gamma)^{24}\text{Mg}$ and $^{23}\text{Na}(p, \alpha)^{20}\text{Ne}$ reactions are presented and the astrophysical implications are discussed.

DOI: 10.1103/PhysRevC.70.045802

PACS number(s): 26.20.+f, 25.10.+s, 25.55.Hp, 98.80.Ft

I. INTRODUCTION

Observations of giant stars in metal-poor globular clusters reveal a number of interesting chemical effects, including a seemingly anomalous anticorrelation between sodium and oxygen (reviewed in [1–4] and references therein). This effect would arise through the simultaneous operation of the CNO and NeNa cycles in which C and O are converted into N while Ne is processed to Na (direct flow from the CNO cycles to the NeNa region is negligible at the temperatures of interest, $T \sim 0.02\text{--}0.08$ GK or $T_9 \sim 0.02\text{--}0.08$). Processed material could then be transported to the stellar surface by deep, nonconvective mixing [5–9], perhaps driven by rotation [10]. However, it is also possible that this “anomaly” actually originated in a previous generation of stars, which then passed this chemical signature down to the stars observed today. In fact, recent observations [11] suggest that both processes may have taken place. A description of either scenario requires an accurate knowledge of the reactions that produce and destroy sodium. Sodium is produced as part of the NeNa cycle (Fig. 1) via the $^{22}\text{Ne}(p, \gamma)^{23}\text{Na}$ reaction, which was the subject of a previous paper (Ref. [12], hereafter Ha01). In the following, we examine the reactions that destroy sodium, namely $^{23}\text{Na}(p, \gamma)^{24}\text{Mg}$ and $^{23}\text{Na}(p, \alpha)^{20}\text{Ne}$.

Low-energy resonances in the $^{23}\text{Na}+p$ system have been studied by Zyskind *et al.* [13] and by Görres *et al.* [14]. Below the lowest observed resonance at $E_{\text{c.m.}}=170$ keV are 4 states, which could correspond to resonances at 5, 37, 138, and 167 keV (as shown in Fig. 2). Neither of the potential resonances at 5 and 167 keV are expected to make a significant contribution to the reaction rate. The former is most likely too low in energy whereas the latter is formed by an angular momentum transfer $\ell=4\text{--}6$ and thus is inhibited by a large centrifugal barrier. Upper limits on the resonance strengths of the remaining 2 states were estimated by El Eid and Champagne [15] who concluded that the 37-keV resonance could contribute to the (p, γ) but not to the (p, α) reaction, with the reverse situation pertaining to the 138-keV resonance. This result is based on a calculation of proton widths using spectroscopic factors estimated from a

(d, n) spectrum of Fuchs *et al.* [16], in which neither state was observed. While it may be possible to detect the 138-keV resonance directly, the 37-keV resonance is too low in energy to be observed in either the (p, α) or (p, γ) channel. In addition, the 170-keV resonance has been observed only in the (p, α) channel [14]. Finally, the high-energy tails of several states just below the $^{23}\text{Na}+p$ threshold could contribute to both reactions. Consequently, we have used the $^{23}\text{Na}(^3\text{He}, d)^{24}\text{Mg}$ reaction to populate states in the vicinity of the $^{23}\text{Na}+p$ threshold. Our procedure is similar to that used by El Eid and Champagne [15] in that we have also estimated proton widths from measured spectroscopic factors. However, because our spectral resolution is improved from that of the previous (d, n) measurement [16], it is possible to make more reliable estimates of the spectroscopic factors for weakly-populated states.

II. EXPERIMENTAL PROCEDURE AND RESULTS

A. Targets

The targets used initially in this work consisted of ^{23}Na implanted into $40\text{-}\mu\text{g}/\text{cm}^2$ $^{\text{nat}}\text{C}$ foils, but these proved to be unstable under bombardment. Subsequent targets consisted of sodium-bearing compounds evaporated onto $20\text{-}\mu\text{g}/\text{cm}^2$ $^{\text{nat}}\text{C}$ foils. Of these, NaF, NaCl, NaI, and Na_2WO_4 either exhibited large backgrounds in the region of interest or degraded with time. However, NaBr was found to be relatively stable and comparatively free of background and thus was used for our measurements. These targets had the lowest oxygen contamination of all of the targets produced, which was particularly important because the ground state and first-excited state of ^{17}F interfere with the states of interest. Two targets were used, with thicknesses (as measured with a deposition monitor) of approximately 49 and $102\text{ }\mu\text{g}/\text{cm}^2$. A third target, consisting of about $16\text{ }\mu\text{g}/\text{cm}^2$ of metallic sodium, sandwiched between thin (about $7\text{ }\mu\text{g}/\text{cm}^2$) layers of gold and on a $20\text{-}\mu\text{g}/\text{cm}^2$ $^{\text{nat}}\text{C}$ foil was also used. This target contained more oxygen than the NaBr target, but was used to verify that any weakly-populated states in ^{24}Mg were not

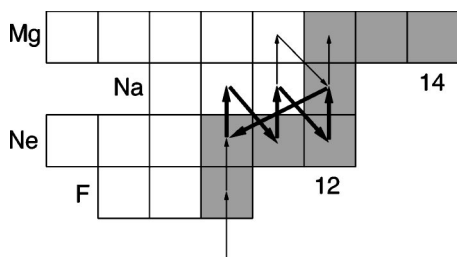


FIG. 1. Integrated fluxes from the CNO cycles up through the NeNa cycle. For the purpose of illustration, we have chosen $T_0 = 0.05$ and $\rho = 100 \text{ g/cm}^3$. Strong flows are indicated by heavy lines and weak flows are represented by dashed lines. Stable nuclei are represented by shaded boxes.

obscured by those arising from $^{78,81}\text{Br}(^3\text{He}, d)^{80,82}\text{Kr}$. In fact, we observed no states that could be attributed to $^{80,82}\text{Kr}$.

B. Experimental details

A 20-MeV $^3\text{He}^{2+}$ beam was provided by the Triangle Universities Nuclear Laboratory FN tandem accelerator, with typical beam currents between 100 and 150 pA. The outgoing deuterons and ^3He were momentum-analyzed with the TUNL Enge Split-Pole Spectrometer and detected using a 42-cm long position-sensitive avalanche counter. The solid angle of the spectrometer was fixed at 2.0 msr in order to reduce the widths of the contaminant lines arising from carbon, nitrogen and oxygen in the target. Data for the $(^3\text{He}, d)$ reaction were collected from $\theta_{\text{lab}} = 5^\circ$ to 22.5° in 2.5° steps and from 25° to 35° in 5° steps. Elastic scattering was measured for $\theta_{\text{lab}} = 5^\circ$ to 45° in 5° steps.

The target was monitored using a ΔE - E silicon telescope, mounted in the target chamber at $\theta_{\text{lab}} = 44.2^\circ$. The aperture of

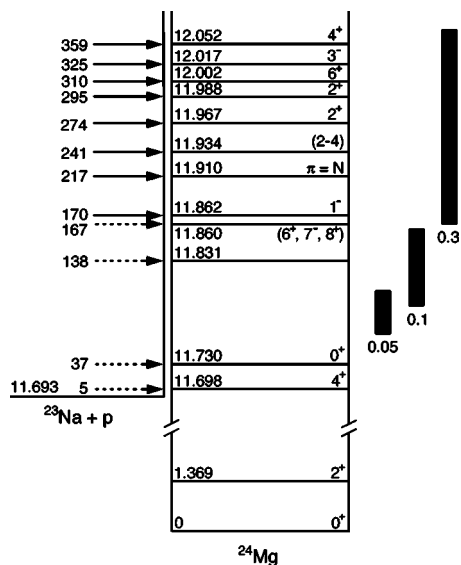


FIG. 2. Energy level diagram for ^{24}Mg . The excitation energies (in MeV) are from this work; spins and parities are taken from Ref. [17]. The corresponding resonance energies are listed in keV (in the center of mass). The Gamow windows corresponding to $T_0 = 0.05$, 0.1, and 0.3 are shown on the right.

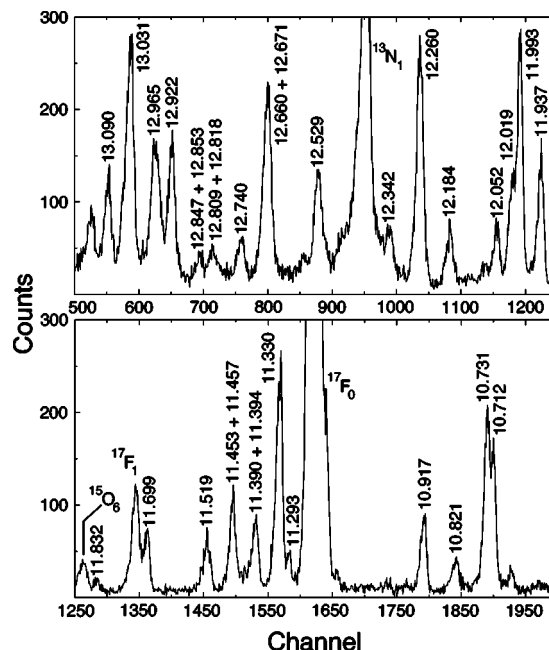


FIG. 3. Deuteron spectrum at $\theta_{\text{lab}} = 12.5^\circ$. The peaks are labeled by either their energy in ^{24}Mg (in MeV) or by the final state formed from a contaminant in the target. Excitation energies are from this study or from Ref. [17]. The latter have been corrected (where appropriate) for a change in the mass of ^{23}Na [18].

the monitor telescope was measured using a calibrated ^{241}Am source and found to be $d\Omega = 0.92 \pm 0.01$ msr, consistent with a geometric measurement of 0.9 ± 0.1 msr. As was the case in Ha01, the yield from elastic scattering measured with the monitor was also used to determine the absolute cross-section scale for the $(^3\text{He}, d)$ data.

III. DATA ANALYSES

A. Excitation energies

A deuteron spectrum collected at $\theta_{\text{lab}} = 12.5^\circ$ is shown in Fig. 3. Following the procedure of Ha01, the deuteron groups were fit with a template consisting of a Gaussian shape with a low-energy exponential tail.

The excitation energies of states observed within about 400 keV of the (p, γ) threshold [$Q = 11.6929(3)$ MeV [18]] were obtained from internal calibrations of the individual deuteron spectra. A total of 12 states above and below the region of interest, with known excitation energies, were used to determine the excitation energies of the intervening levels. These states are noted in Fig. 3 and were chosen because they correspond to well-resolved peaks in the deuteron spectra (the 12.260-MeV peak is in fact a close doublet of states differing in energy by 0.4 keV [17], which we treated as a single level). Where necessary, the energies of the calibration states were corrected using the updated value for the mass of ^{23}Na [18]. A third-order polynomial was used to fit the E_x vs channel number data. Based on predicted energies of states not used in the calibration process, the error in our excitation energies was estimated to be ± 2 keV for $\theta \leq 10^\circ$ and ± 3 keV for $\theta \geq 12.5^\circ$. The adopted excitation energies (shown in

TABLE I. Adopted excitation energies (MeV).

This study	Literature						Adopted
	a	b	c	d	e	f	
11.6986(13)		11.694(3)		11.699(2)			11.6982(10)
		11.727(3)		11.731(2)			11.7298(17)
11.8317(18)		11.828(3)					11.8307(15)
	11.860(3)						11.860(3)
11.8627(12)		11.862(3)	11.861(4)	11.868(3)		11.8597(20)	11.8624(9)
			11.907(4)			11.9104(20)	11.9097(18)
11.9365(12)		11.935(3)			11.9333(4)	11.9334(10)	11.9336(4)
11.9653(12)		11.967(3)	11.967(4)	11.974(3)	11.9669(6)	11.9670(10)	11.9669(5)
11.9929(12)		11.989(3)			11.9880(3)	11.9890(10)	11.9883(3)
		12.002(3)	12.003(4)				12.0024(24)
12.0190(12)		12.015(3)	12.016(4)		12.0174(7)	12.0168(10)	12.0174(5)
12.0518(12)		12.050(3)	12.050(4)		12.0516(6)		12.0516(5)

^aReference [19].

^bReference [20].

^cReference [21].

^dReference [22].

^eReference [17].

^fReference [14].

Table I) are a weighted average of the present results and all previous data.

Two of the 8 states listed in Table I correspond to the potential $^{23}\text{Na}+p$ resonances at $E_{\text{c.m.}}=5$ and 138 keV (corresponding to $E_x=11.698$ and 11.831 MeV, respectively). The remaining states correspond to the 6 lowest observed resonances. No evidence was seen for $E_x=11.730$ and 11.860-keV states, which would correspond to the remaining possible resonances at 37 or 167 keV, respectively. Therefore, neither state possesses significant single-particle strength. As mentioned above, the relatively high spin of the latter state precludes it from having astrophysical significance. On the other hand, the former state has $J^\pi=0^+$ and can be formed via d -wave proton capture. However, if this state is primarily rotational in character, it would be expected to be weakly excited in the $(^3\text{He}, d)$ reaction, which is the case for the known $J^\pi=0^+$ bandheads [23].

B. Angular distributions

The analysis of the angular-distribution data also follows the procedure described in Ha01. Briefly, absolute cross sections were determined relative to that for elastic scattering, measured with the monitor detector. Theoretical differential cross sections were calculated with the DWBA code DWUCK4 [24]. The $^{23}\text{Na}+^3\text{He}$ potential parameters were based on the global parametrization of Becchetti and Greenlees [25], with modifications to improve the fit to our elastic-scattering data (shown in Fig. 4). Deuteron potentials were derived from the global parametrization of Daehnick *et al.* [26]. A summary of these parameters is given in Table II. Unbound form factors were calculated for the states above the $^{23}\text{Na}+p$ threshold.

The relationship between the measured differential cross

section, $d\sigma/d\Omega_{\text{exp}}$, and that calculated by DWUCK4, $d\sigma/d\Omega_{\text{DWBA}}$, is

$$\left(\frac{d\sigma}{d\Omega}\right)_{\text{exp}} = N \frac{(2J_f + 1)}{(2J_i + 1)(2j + 1)} C^2 S \left(\frac{d\sigma}{d\Omega}\right)_{\text{DWBA}}, \quad (1)$$

where $N=4.42$ is an overall normalization [28], J_f and J_i are the spins of the final and initial states, respectively, and j is the transferred total angular momentum. In this case, $j = \ell \pm 1/2$, where ℓ is the transferred orbital angular momentum. We assumed $2s_{1/2}$, $2p_{3/2}$, $1d_{5/2}$, and $1f_{7/2}$ transfer. The quantity C^2S is the spectroscopic factor (the isospin Clebsch-Gordan coefficient $C^2=1/2$ for both $T=0$ states and $T=1$

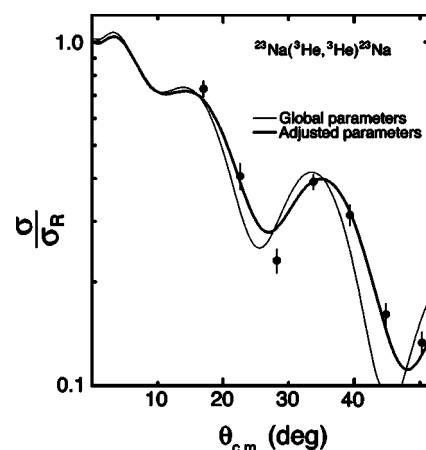


FIG. 4. The ratio of the differential cross section for $^{23}\text{Na}(^3\text{He}, ^3\text{He})^{23}\text{Na}$ to that for Rutherford scattering. The fits are DWBA calculations using different optical model parameters, as described in the text.

TABLE II. Optical model parameters.

Particle	V_r	r_r	a_r	W_i	W_D	$r_i=r_D$	$a_i=a_D$	V_{so}	r_{so}	a_{so}	r_c
${}^3\text{He}^a$	159.3	1.05	0.72	42.12		1.33	0.86				1.30
d^b	88.6	1.17	0.73	0.24	36.1	1.33	0.73	13.86	1.07	0.66	1.30
p^c	^d	1.17	0.69					$\lambda=25$			1.28

^aFrom Ref. [25] and present elastic scattering data.

^bReference [26].

^cReference [27].

^dVaried to match separation energy.

states). For unbound states, the proton width, Γ_p can be obtained via

$$\Gamma_p = C^2 S \Gamma_{sp}, \quad (2)$$

where Γ_{sp} is the proton width for a pure single-particle state, calculated directly by DWUCK4.

Analogous expressions can be written for the cross section and proton width by using asymptotic normalization coefficients rather than spectroscopic factors. Although the former is inherently less sensitive to the parameters used to describe the bound-state potential, we have adopted the latter formulation for ease of comparison with previous results. However, the proton width derived from either asymptotic normalization coefficients or spectroscopic factors is quite insensitive to the choice of nuclear potential [29], as we will illustrate below.

The angular distributions for the 12 calibration states are shown in Fig. 5. In Fig. 6, we show the angular distributions for the states near the proton-capture threshold. We have also included 95%-CL upper limits for the (unobserved)

11.730-MeV state. These were derived from the statistics of the background using the technique of maximum-likelihood estimation with Poisson statistics [30]. Spectroscopic factors were obtained by a least-squares fit of the DWBA cross sections to the data and are listed in Table III. The $1-\sigma$ statistical uncertainty in the fitting procedure is about 6% for states formed primarily by a single ℓ -transfer and about 10% for strongly mixed states. There are also systematic uncertainties arising from the choice of optical-model parameters. Since the absolute cross sections were determined relative to elastic scattering, C^2S is proportional to the ratio of the DWBA prediction for (${}^3\text{He}, {}^3\text{He}$) to that for (${}^3\text{He}, d$). Hence, uncertainties in the ${}^3\text{He}$ parameters are the major contributors to the systematic uncertainty. By varying the ${}^3\text{He}$ parameters within a reasonable range, we estimate that the uncertainty associated with the ${}^3\text{He}$ parameters alone is 26%. Similar comparisons using different sets of deuteron parameters produce an average deviation of about 11%. There is also a small (2.5%) uncertainty in the fit to the elastic-scattering data. Finally, we have adopted a theoretical uncertainty of 15% in the normalization factor N , as discussed in

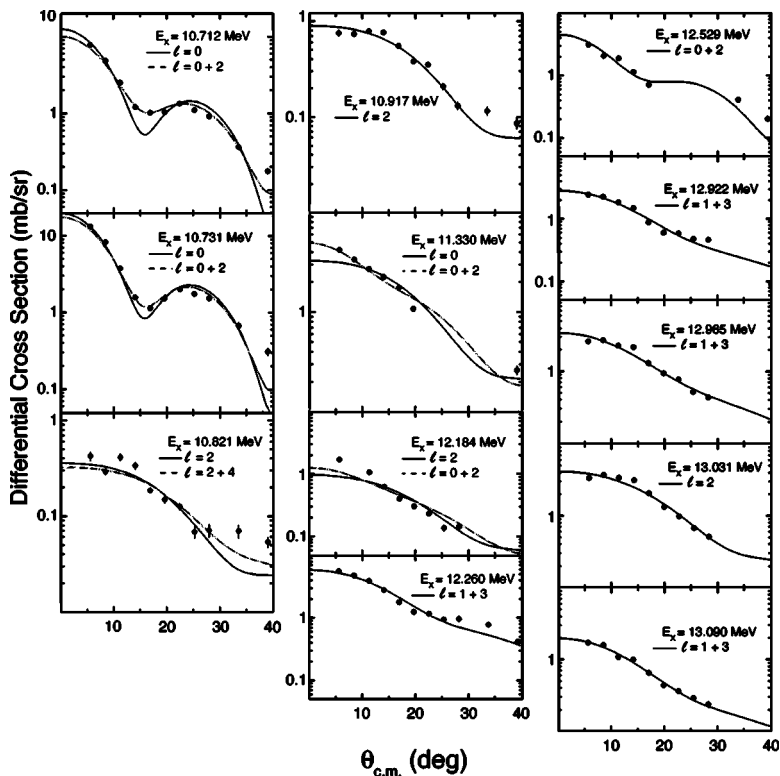


FIG. 5. Angular distributions and DWBA fits for the 12 reference states. The error bars on the data points reflect statistical uncertainties only. The orbital angular momentum transfer is noted for each fit.

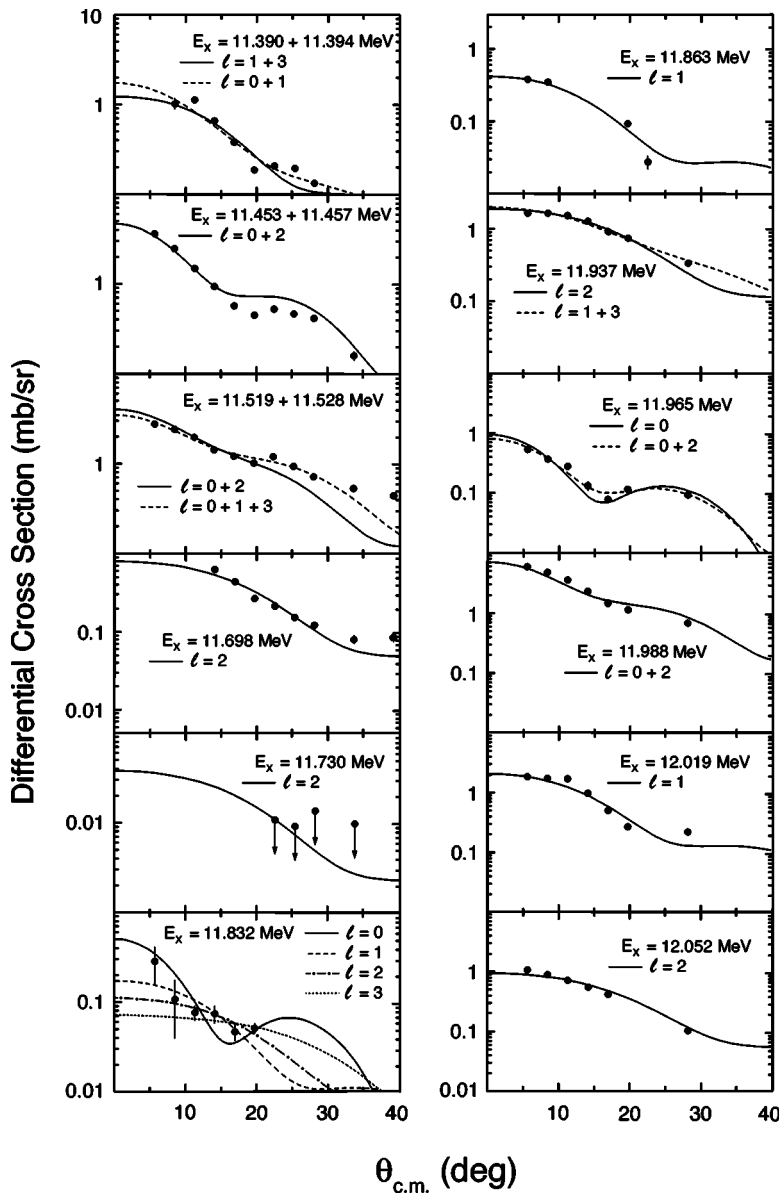


FIG. 6. Angular distributions and DWBA fits for states corresponding to possible low-energy resonances. The orbital angular momentum transfer is noted for each fit.

Ref. [29]. Although this uncertainty has normally not been considered separately in previous work, we do so here for completeness, and to illustrate that it is significant. Treating all of these uncertainties as independent, Gaussian-distributed errors implies a total uncertainty of 33% for the spectroscopic factors reported here. This result does not include any uncertainty associated with the bound-state potentials. Since these parameters are not well-constrained by experiment, it is difficult to make a quantitative estimate of the associated uncertainty, which can be quite significant. Hence, the spectroscopic factors listed in Table III should be considered as valid for our particular choice of bound-state parameters and comparisons with other data are only meaningful if this source of systematic error is taken into account. However, this uncertainty does not enter significantly into the calculation of the proton width, provided that the single-particle width is calculated using the same bound-state wave function.

As discussed by Bertone *et al.* [29], both C^2S and Γ_{sp} are strongly dependent on the bound-state potential, but their

variations are anticorrelated. A deep potential with a correspondingly large amplitude for the interior wave function yields a smaller spectroscopic factor than is the case for a shallower potential with a smaller interior amplitude. On the other hand, a deeper potential will result in a larger value for Γ_{sp} , which depends upon the value of the wave function at the interaction radius. These variations are largely cancelled in the product $C^2S \times \Gamma_{sp}$; thus Γ_p is rather insensitive to the choice of parameters for the bound-state potential. To illustrate this point, we have calculated proton widths for a fictitious d -wave resonance at $E_{c.m.} = 200$ keV using our adopted values for radius and diffuseness, $r_r = 1.17$ fm and $a_r = 0.69$ fm, and for $r_r = 1.35$ fm, $a_r = 0.5$ and 0.8 fm. For this range of parameters, the maximum deviation in Γ_p from the value derived using our canonical parameters is 3.3%. A second source of systematic error in Γ_p arises from ambiguity in the transferred angular momentum for $l > 0$ transfer. For example, a 0^+ state can be formed by $l = 2$ transfer with $J = 3/2$ or $5/2$. For such a state at $E_{c.m.} = 200$ keV, the resulting spectroscopic factors would differ by about 20%, but the

TABLE III. Summary of spectroscopic factors.

E_x (MeV) ^a	J^π ^b	ℓ	$(2J_f+1)C^2S$	
			This study ^c	Literature
10.712	1 ⁺	0	0.53	^e
		0+2	0.38+0.16	
10.731	2 ⁺	0	0.84	^e
		0+2	0.72+0.12	
10.821	3 ⁺	2	0.057	0.13(5) ^f
		2+4	0.050+0.035	
10.917	2 ⁺	2	0.14	0.18(6) ^f
11.330	(2-4) ⁺	2	0.48	
		0+2	0.13+0.40	
11.390	1 ⁻	1	(0.06)	0.24 ^g
11.453 ^d	2 ⁺	0	0.24	^h
11.457 ^d	0 ⁺	2	0.16	^h
11.519	2 ⁺	0	(0.10)	0.12 ^g
11.698	4 ⁺	2	0.11	
		2+4	0.097+0.043	
11.730	0 ⁺	2	≤ 0.0067	
11.831	?	0	0.039	
		1	0.0090	
		2	0.015	
		3	0.024	
11.862	1 ⁻	1	0.026	
11.934	(2-4)	2	0.25	
		0+2	0.021+0.24	
		1+3	0.085+0.20	
		2+4	0.23+0.13	
11.967	2 ⁺	0	0.084	
		0+2	0.064+0.012	
11.988	2 ⁺	0+2	0.42+0.33	
12.017	3 ⁻	1	0.13	
12.052	4 ⁺	2	0.13	
12.184	(1,2) ⁺	2	0.13	
		0+2	0.048+0.11	
12.260 ^d	2 ⁻ , 3 ⁻	1+3	0.35+0.28	
12.529	1 ⁺	0+2	0.57+0.12	
12.922	3 ⁻	1+3	0.21+0.13	
12.965	2 ⁻	1+3	0.31+0.19	
13.031	2 ⁺	2	0.56	
13.090	3 ⁻	1+3	0.17+0.073	

^aAdopted energies from this study and from Ref. [17]. The latter have been corrected (where appropriate) for the revised mass of ²³Na.

^bReference [17].

^cThese values have an overall uncertainty of 33%.

^dUnresolved doublet.

^eUnresolved doublet in Refs. [16,23] with $(2J_f+1)C^2S=1.3(4)$ ($\ell=0$) and $1.2(6)+0.48(24)$ ($\ell=0+2$), respectively.

^fReference [23].

^gReference [16].

^hUnresolved doublet in Refs. [16,31] with $(2J_f+1)C^2S(\ell=0)=0.32$ and 0.13, respectively.

TABLE IV. Comparison of proton widths.

E_x (MeV)	E_{cm} (keV)	J^π	ℓ	$(2J_f+1)\Gamma_p$ (eV)	
				$(^3\text{He}, d)$	Literature ^a
11.862	169.5	1 ⁻	1	$1.6(5) \times 10^{-4}$	$1.83(39) \times 10^{-4}$
11.934	240.7	(2-4)	2	$2.5(9) \times 10^{-3}$	$(3.1-6.7) \times 10^{-3b}$
11.967	274.0	2 ⁺	0+2	0.46(16)	0.28(3)
11.988	295.4	2 ⁺	0+2	6.2(21)	1.1(2) ^c
12.017	324.5	3 ⁻	1	1.1(4)	0.59(28)
12.052	358.7	4 ⁺	2	0.076(26)	0.044(12)
12.922	1229	3 ⁻	1+3	$1.4(5) \times 10^4$	$4.6(5) \times 10^4$ $4.2(4) \times 10^{4d}$
12965	1272	2 ⁻	1+3	$1.9(6) \times 10^4$	$1.5(2) \times 10^{4d}$
13031	1338	2 ⁺	2	$3.6(12) \times 10^3$	$\ell=0: 2.0(2) \times 10^{3d}$ $\ell=2: 7.0(7) \times 10^{3d}$
13090	1397	3 ⁻	1+3	$1.9(6) \times 10^4$	$\ell=1: 3.9(4) \times 10^{4d}$ $\ell=3: 1.8(2) \times 10^{3d}$

^aReference [17] and references therein, unless otherwise noted.

^bUsing $\Gamma_p/\Gamma > 0.7$ from Ref. [32].

^cUsing $\Gamma_p/\Gamma = 0.70(9)$ from Ref. [32].

^dReference [37].

proton widths would differ by only 5%. Assuming uncertainties of 5% arising from both the bound-state potential and the choice of transferred angular momentum, combined with a 33% uncertainty for the spectroscopic factor results in an overall uncertainty of 34% for our predicted proton widths.

For 10 states, it is possible to compare the proton widths calculated as described above with values derived from previous experiments. The latter were obtained from measurements of Γ [21,22], Γ_γ/Γ [32], (p, γ) [14,17], (p, α) [13,14,33-35], and (α, γ) [22,36] resonance strengths, and (p, p) measurements [37]. The (p, α) resonance strengths have been corrected for changes in target stoichiometry, which is discussed in more detail in Sec. IV. The results are listed in Table IV. There is agreement within experimental uncertainties for 6 states, but there are also a number of significant discrepancies, which may arise from our choice of a simple potential model to describe these states. To further evaluate the usefulness of this technique, we have examined states in the sd -shell with measured Γ_p and C^2S . We have restricted our attention to states with known J^π , located within 2 MeV of the proton-capture threshold. These requirements were designed to ensure that reliable unbound form factors could be calculated. In addition we limited our sample to states with Γ less than about 20 keV, so that the width would be well defined. Finally, we ignored mixed- ℓ transitions in which the strength of the lowest ℓ -component could not be extracted from the angular distribution. Where necessary, we have derived new values of C^2S using unbound form factors. A total of 72 states were surveyed in $^{21,23}\text{Na}$ [12,38], ^{24}Mg (this study), $^{25,26,27}\text{Al}$ [39-41] ^{28}Si [42], $^{29,31}\text{P}$ [43,44], ^{32}S [45], ^{33}Cl [46], and ^{41}Sc [47]. Proton widths were obtained from the original references and from Ref. [17]. For each state, we have calculated the ratio of Γ_p derived from $\text{C}^2\text{S} \cdot \Gamma_p(\text{calc})$ to the experimental value. The natural logarithm of this ratio is approximately Gaussian,

with a mean value of 0.14 and a standard deviation of 0.47 (Fig. 7). This implies that $\text{C}^2\text{S} \cdot \Gamma_p(\text{calc})$ has a log-normal probability distribution, with a 1- σ uncertainty of a factor of 1.6. We have adopted this latter value for our calculations of Γ_p .

IV. ASTROPHYSICAL ASPECTS

A. General considerations

The thermonuclear reaction rate is $N_A \langle \sigma v \rangle$, where N_A is Avagadro's number and $\langle \sigma v \rangle$ is the thermally-averaged product of total cross section and velocity (in the center of mass). The contribution from an isolated, narrow resonance at $E_{\text{c.m.}}$ can be written as

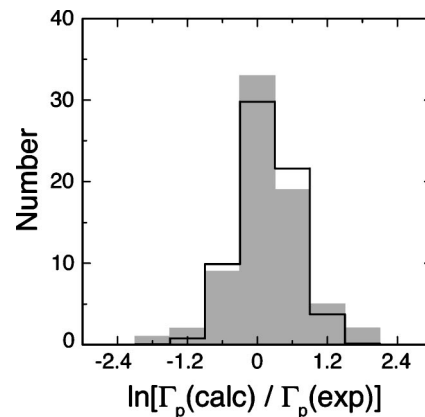


FIG. 7. The shaded area is a histogram of $\ln[\Gamma_p(\text{calc})/\Gamma_p(\text{exp})]$, where $\Gamma_p(\text{calc})$ is the proton width derived from C^2S and $\Gamma_p(\text{exp})$ is the experimentally-determined value. The solid line is a Gaussian fit with a mean value of 0.14 and a standard deviation of 0.47. The binning reflects an overall uncertainty in C^2S of about 30%.

TABLE V. Strengths of low-energy resonances.

E_x^a	E_{cm}^a	J^π	$\omega\gamma$ (eV) ^c		$\omega\gamma$ (eV)-recommended ^d	
			(p, γ)	(p, α)	(p, γ)	(p, α)
11.698	5.3	4 ⁺	$(0.85-3.0) \times 10^{-56}$	$(1.2-3.0) \times 10^{-55}$	1.6×10^{-56}	1.9×10^{-55}
11.730	36.9	0 ⁺	$\leq 1.3 \times 10^{-24}$	$\leq 3.3 \times 10^{-20}$	$\leq 1.3 \times 10^{-24}$	$\leq 3.3 \times 10^{-20}$
11.831	137.8	?	$\ell=0: (5.4-14) \times 10^{-6}$ $\ell=1: (2.6-6.6) \times 10^{-7}$ $\ell=2: (0.94-2.4) \times 10^{-8}$ $\ell=3: (1.8-4.6) \times 10^{-10}$	$\leq 1.6 \times 10^{-6}$ $\leq 7.5 \times 10^{-8}$ $\leq 2.8 \times 10^{-9}$ $\leq 5.4 \times 10^{-11}$	$1.5 \leq 10^{-8}$	$\leq 2.8 \times 10^{-9}$
11.862	169.5	1 ⁻	$1.2(4) \times 10^{-9}$	$2.3(4) \times 10^{-5e}$	1.20×10^{-9}	2.3×10^{-5}

^aExcitation energies (in MeV) are from Table I. Resonance energies are in keV.

^bReference [17].

^cThe 68% confidence band is listed; upper limits are quoted at a 95% confidence level.

^dValue used for the recommended rate.

^eFrom Refs. [13,14], corrected for target stoichiometry.

$$\langle\sigma v\rangle = \left(\frac{2\pi}{\mu kT}\right)^{3/2} \hbar^2 (\omega\gamma)_r \exp\left(-\frac{E_{\text{cm}}}{kT}\right). \quad (3)$$

The quantity μ is the reduced mass, k is Boltzmann's constant, and $\omega\gamma$ is the resonance strength, defined by

$$\omega\gamma = \frac{2J_r + 1}{(2J_t + 1)(2J_p + 1)} \frac{\Gamma_p \Gamma_o}{\Gamma}, \quad (4)$$

in which J_r , J_t , and J_p are the spins of the resonance, target and incident proton, respectively. The quantity Γ_o refers to the partial width of the outgoing channel; in this case $\Gamma_o = \Gamma_\gamma$ or Γ_α ; $\Gamma = \Gamma_p + \Gamma_\gamma + \Gamma_\alpha$ is the total width. For situations where the tails of resonances are important, or if the resonances are broad, $\langle\sigma v\rangle$ must be evaluated numerically. In the following, we will discuss the values that we have adopted for the strengths of the low-energy resonances, which are summarized in Table V.

B. Resonance strengths

1. Subthreshold resonances

Although any state in the vicinity of the $^{23}\text{Na}+p$ threshold could contribute to the reaction rate as a subthreshold resonance, in practice the $2s_{1/2}$ states nearest threshold usually have the major impact. Two such states exist within about 300 keV of threshold: $E_x=11.453$ MeV ($J^\pi=2^+$), and 11.519 MeV ($J^\pi=2^+$). In addition, the 11.390-MeV state ($J^\pi=1^-$) could be a p -wave subthreshold resonance. These states appear as components of unresolved doublets in our deuteron spectra. The 11.390-MeV state appears in combination with the 11.394-MeV state (J^π unknown). The $\ell=1$ component of the combined angular distribution (Fig. 6) yields $C^2S(\ell=1) \approx 0.02$. The 11.453-MeV state is combined with the 11.457-MeV (0^+) state. An $\ell=0+2$ fit to the angular distribution for this pair suggests $C^2S(\ell=0) \approx 0.05$, which would be associated with the 11.453-MeV state. Similarly, the angular distribution for the 11.519-MeV+11.528-MeV states was best fit with $\ell=0+1+3$, yielding $C^2S(\ell=0) \approx 0.02$ for the 11.519-MeV state.

In order to calculate the impact that these states would have on either the (p, γ) or (p, α) reactions, we have derived values for Γ_γ and Γ_α from measurements of (α, γ) resonance strengths [22,36], total widths [17], and γ -ray branching ratios [32]. We find that the subthreshold resonances have a negligible impact on the (p, γ) rate, which is dominated by direct capture at low temperatures. This is in disagreement with the recent Nuclear Astrophysics Compilation of Reaction Rates (NACRE) tabulation [48]. However, this earlier work did not include the direct-capture component. In contrast, the subthreshold resonances do contribute to the (p, α) reaction. Unfortunately, it is only possible to derive a lower limit for the reduced α width of the 11.453-MeV state. Therefore, we have neglected this state in our calculation of the rate from subthreshold resonances.

2. $E_x=11.698$ MeV; $E_{\text{c.m.}}=5$ keV

The 11.698-MeV state was rather strongly populated and $\ell=2$ transfer is indicated. The value of $C^2S=0.012$ implies $\Gamma_p=1.8 \times 10^{-55}$ eV. Vermeer *et al.* [32] have measured $\Gamma_\gamma/\Gamma=0.08(3)$, which implies $\Gamma_\alpha/\Gamma=0.92(3)$ (hereafter, we will denote these branching ratios by B_γ and B_α , respectively). From these values, we obtain $\omega\gamma=1.6 \times 10^{-56}$ eV for the (p, γ) reaction and 1.9×10^{-55} eV for the (p, α) reaction. As discussed above, Γ_p follows a log-normal probability distribution whereas we assume normal distributions for B_γ and B_α . Thus, the respective standard deviations cannot be combined in the usual manner. Therefore, to determine an overall uncertainty, we have explicitly calculated the probability distribution for $\omega\gamma$. For the (p, γ) reaction, a 68% confidence belt would include $\omega\gamma=0.85-3.0 \times 10^{-56}$ eV. Similarly, for the (p, α) reaction, we obtain $\omega\gamma=1.2-3.0 \times 10^{-55}$ eV. Neither resonance strength is astrophysically significant.

3. $E_x=11.730$ MeV; $E_{\text{c.m.}}=37$ keV

As mentioned above, no evidence for the 11.730-MeV state was observed at any angle. Since $J^\pi=0^+$, the minimum ℓ -transfer is $\ell=2$. Assuming a pure, direct process, $C^2S \leq 0.0067$ and $\Gamma_p \leq 1.3 \times 10^{-19}$ eV (both 95% confidence lim-

TABLE VI. Corrected (p, α) resonance strengths.

E_{cm} (keV)	$\omega\gamma$ (eV)							Adopted ^a
	b	c	d	e	f	g	h	
169.5					2.5(6)e-5	2.1(6)e-5		2.3(4)e-5
217.5						5.4(13)e-5		5.4(13)e-5
240.6			≤ 0.1					≤ 0.1
273.9	0.036(10)	0.038(6)	0.077(16)			0.031(7)		0.035(4)
295.3	$\leq 4.4\text{e-}3$		≤ 0.064					$\leq 4.4\text{e-}3$
324.4	0.054(14)	0.070(12)	0.10(2)			0.075(16)	0.0716(29)	0.071(2)
358.6		4.1(10)e-3	≤ 0.012					4.1(10)e-3
426.3		5.7(14)e-3	≤ 0.02					5.7(14)e-3
490.6	≤ 0.011		≤ 0.08					≤ 0.011
566.8	34(7)		33(7)		40(3)			38(3)
648.0	≤ 0.041		≤ 0.15					≤ 0.041
692.6			≤ 0.25					≤ 0.25
707.9			≤ 0.12					≤ 0.12
712.6			6.9(14)	9.9(30)				7.4(13)
761.6			3.2(6)	3.6(11)				3.3(5)
778.9			1.7(3)	2.3(7)				1.8(3)
809.5			0.51(10)					0.51(10)
880.4				63(26)				63(26)
968.2				46(14)				46(14)

^aWeighted average of individual values.

^bCalculated from α -yields of Ref. [33].

^cCalculated from α -yields of Ref. [34].

^dCalculated from α -yields of Ref. [35]. Upper limits are at the 1- σ level.

^eReference [53]. These results appear to be systematically high and were normalized to the adopted value at $E_{\text{cm}}=566.8$ keV. A target of NaCN was used, thus there are no corrections for stoichiometry.

^fFrom relative measurement of Ref. [13] using adopted strength for $E_{\text{cm}}=273.9$ keV.

^gReference [14], corrected for stopping power.

^hReference [51].

its). The latter is a factor of 38 below the previously-accepted limit [15]. The other partial widths have been tabulated [17]: $\Gamma_{\gamma}=0.37(6)$ eV and $\Gamma_{\alpha}\approx\Gamma=10(2)$ keV. From this information, we obtain $\omega\gamma_{(p,\gamma)}\leq 1.3\times 10^{-24}$ eV and $\omega\gamma_{(p,\alpha)}\leq 3.3\times 10^{-20}$ eV, which are both 95% confidence limits. As a result, this resonance has a negligible impact on the (p, γ) reaction, but may contribute to the (p, α) reaction over a fairly narrow range of temperatures, $T_9\approx 0.015-0.02$. Since this state does not make a significant contribution to either reaction, we have ignored it in arriving at recommended reaction rates.

4. $E_x=11.831$ MeV; $E_{\text{c.m.}}=138$ keV

The 11.831-MeV state was partially obscured at $\theta_{\text{lab}}\leq 7.5^\circ$ by nitrogen contamination in the target backing. In addition, no angular-distribution data could be obtained for $\theta_{\text{lab}}> 17.5^\circ$ because of contaminant groups arising from oxygen. However, the magnitude of the partial angular distribution that we have obtained is consistent with a direct-reaction process. Unfortunately, the spin and parity of this state are not known and the shape of the angular distribution alone

does not unambiguously establish the ℓ -transfer. This state would correspond to an astrophysically-significant resonance for $\ell\leq 3$ and thus we have determined proton widths for $\ell=0-3$. These, combined with $B_{\gamma}=0.95(4)$ [32] determine a range of (p, γ) resonance strengths. However, since our data do not rule out the possibility of $\ell>3$ transfer or a significant contribution from a nondirect process, we have used the $\ell=0$ result as an upper limit. In this case, our 68% confidence range is 5.4–14 μeV , with a central value of 8.6 μeV . These values are somewhat larger than the previous upper limit of 5 μeV [14], which was quoted without a confidence level. Assuming that this limit was at a 1- σ level and that the statistics are Gaussian, the resulting 95% confidence limit would be 8.2 μeV , which is smaller than our maximum value of 14 μeV . However, if the statistics in the previous study are better described by a Poisson distribution, then the 95% confidence limit could be larger than 8.2 μeV . To be conservative, we have adopted our value of 14 μeV in calculating the maximum reaction rate. A direct search for this resonance has recently been carried out [49], which yields $\omega\gamma\leq 0.15$ μeV . If this result is verified, then it would rule out s -wave capture for this resonance.

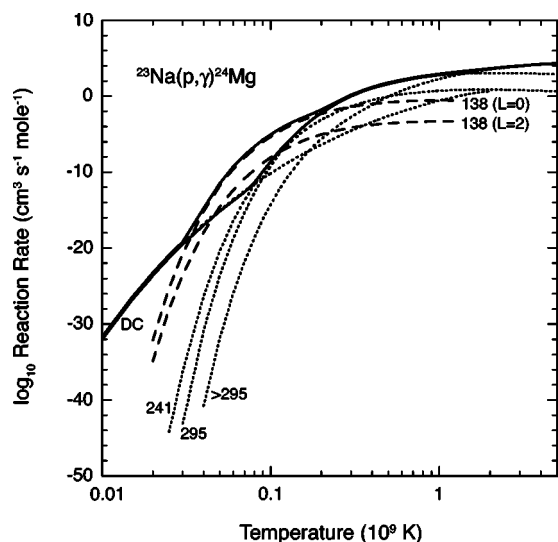


FIG. 8. Total reaction rate (solid lines), and individual contributions of resonances and direct capture (dotted lines) for the $^{23}\text{Na}(p, \gamma)^{24}\text{Mg}$ reaction. The upper limit ($L=0$) and recommended ($L=2$) value for the 138-keV resonance are represented by dashed lines.

The branching ratio for α -decay, $B_\alpha=0.05(4)$, is only marginally significant and so we have treated it as an upper limit. Since the standard deviation is comparable to the central value, we have used log-normal statistics to describe B_α . For $\ell=0$, $\omega\gamma_{(p,\alpha)} \leq 1.6 \mu\text{eV}$ (95% C.L.). This is larger than the published upper limit $\omega\gamma_{(p,\alpha)} \leq 0.5 \mu\text{eV}$ from Ref. [14] but again it is not clear how to quote a comparable confidence limit. Consequently, we have used $\omega\gamma_{(p,\alpha)} \leq 1.6 \mu\text{eV}$ to calculate the maximum reaction rate.

5. $E_x=11.862 \text{ MeV}$; $E_{\text{c.m.}}=169.5 \text{ keV}$

The 11.862-MeV state has been observed as a resonance in the (p, α) and (α, γ) reactions [13,14,22,36], but not in the (p, γ) reaction. However, since this state appears to possess some single-proton strength, it must also be a (p, γ) resonance. Our value of $C^2S=8.7 \times 10^{-3}$ implies $\Gamma_p=53 \mu\text{eV}$. From $\omega\gamma_{(\alpha,\gamma)}=1.0(2) \text{ eV}$ [22], $\omega\gamma_{(p,\alpha)}=23(5) \mu\text{eV}$ [13,14] and $\Gamma=7.0(3) \text{ keV}$ [21], we find $\Gamma_p=61(13) \mu\text{eV}$ and $\Gamma_\gamma=0.37(7) \text{ eV}$. These values yield $\omega\gamma_{(p,\gamma)}=1.20(35) \text{ neV}$, which has a negligible impact on the (p, γ) reaction rate.

6. Low-energy (p, α) resonances

Most direct measurements of low-energy (p, α) resonances have used NaCl targets, for which a stoichiometry Na:Cl=1:1 was assumed. However, after a very short period of bombardment, the stoichiometry will change to an approximately constant value Na:Cl \approx 5:3 [50]. Thus, the effective stopping powers used to convert the measured reaction yields into resonance strengths are in error. The net effect is that the published resonance strengths are about 30% too large [51]. Three of the existing measurements [33–35] quote alpha yields explicitly and so we have recalculated the resonance strengths using stopping powers ob-

TABLE VII. $^{23}\text{Na}(p, \gamma)^{24}\text{Mg}$ reaction rate.

T_9	Low	Recommended	High
0.010	9.03e-33	1.35e-32	2.02e-32
0.015	1.34e-27	2.01e-27	2.99e-27
0.020	2.45e-24	3.65e-24	5.45e-24
0.025	5.06e-22	7.55e-22	1.13e-21
0.030	2.94e-20	4.39e-20	6.46e-20
0.040	1.02e-17	1.64e-17	1.69e-15
0.050	6.80e-16	3.63e-15	3.32e-12
0.060	1.67e-14	4.40e-13	5.04e-10
0.070	2.34e-13	1.53e-11	1.76e-08
0.080	4.36e-12	2.20e-10	2.48e-07
0.090	1.27e-10	1.80e-09	1.90e-06
0.10	2.57e-09	1.12e-08	9.52e-06
0.11	3.66e-08	6.71e-08	3.52e-05
0.12	2.91e-07	4.13e-07	1.03e-04
0.13	1.90e-06	2.36e-06	2.56e-04
0.14	9.76e-06	1.16e-05	5.55e-04
0.15	4.09e-05	4.77e-05	1.09e-03
0.16	1.44e-04	1.68e-04	1.99e-03
0.18	1.20e-03	1.40e-03	5.92e-03
0.20	6.52e-03	7.67e-03	1.71e-02
0.25	1.35e-01	1.61e-01	2.14e-01
0.30	9.89e-01	1.18e+00	1.46e+00
0.35	3.98e+00	4.73e+00	5.76e+00
0.40	1.10e+01	1.31e+01	1.59e+01
0.45	2.40e+01	2.86e+01	3.42e+01
0.50	4.40e+01	5.25e+01	6.27e+01
0.60	1.07e+02	1.28e+02	1.52e+02
0.70	2.01e+02	2.38e+02	2.83e+02
0.80	3.22e+02	3.79e+02	4.48e+02
0.90	4.70e+02	5.49e+02	6.41e+02
1.0	6.48e+02	7.46e+02	8.62e+02
1.3	1.36e+03	1.51e+03	1.69e+03
1.5	1.98e+03	2.17e+03	2.39e+03
1.8	3.14e+03	3.39e+03	3.65e+03
2.0	4.07e+03	4.35e+03	4.66e+03
2.5	6.71e+03	7.13e+03	7.58e+03
3.0	9.65e+03	1.02e+04	1.09e+04
3.5	1.26e+04	1.34e+04	1.42e+04
4.0	1.53e+04	1.63e+04	1.74e+04
5.0	1.97e+04	2.11e+04	2.25e+04

tained from SRIM2000 [52] for Na:Cl \approx 5:3. The remaining 2 studies that used NaCl targets [13,14] list resonance strengths only and so these were corrected by multiplying them by the appropriate ratio of stopping powers. We have assigned uncertainties of $\pm 15\%$ to the absolute stopping powers and $\pm 10\%$ to the relative stopping powers. Finally, the yields of Ref. [33] do not include corrections for angular distributions. We have accounted for this effect by using an average of the angular-distribution coefficients reported by

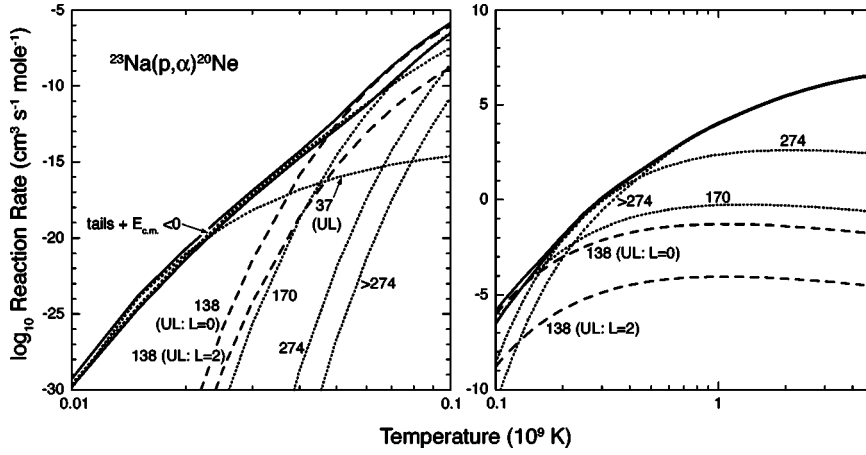


FIG. 9. Total reaction rate (solid lines), and the contributions of individual resonances (dotted lines) for the $^{23}\text{Na}(p, \alpha)^{20}\text{Ne}$ reaction. The upper limits for $L=0$ and $L=2$ capture into the 138-keV resonance are represented by dashed lines.

Refs. [34,35,53]. We list the corrected resonance strengths and our recommended values in Table VI.

C. Reaction rates

1. The $^{23}\text{Na}(p, \gamma)^{24}\text{Mg}$ reaction

For $T_9 \leq 5$, the rate for the $^{23}\text{Na}(p, \gamma)^{24}\text{Mg}$ reaction is dominated by direct capture and by the contributions of individual resonances. We have calculated the cross section for direct capture, σ^{DC} in the $^{23}\text{Na}(p, \gamma)^{24}\text{Mg}$ reaction using the familiar relation

$$\sigma^{\text{DC}} = C^2S \sigma_{\text{th}}^{\text{DC}}, \quad (5)$$

where $\sigma_{\text{th}}^{\text{DC}}$ is the calculated cross section for a pure single-particle state. Spectroscopic factors were taken from this work and from values tabulated in Ref. [17]. Calculations of $\sigma_{\text{th}}^{\text{DC}}$ were performed using the same bound-state potential parameters as were used to extract C^2S . In cases where there are several values for C^2S for a given state, we have averaged the resulting σ^{DC} . The spread in the individual σ^{DC} suggest an overall uncertainty of 40% for the direct-capture rate. Converting σ^{DC} into an astrophysical S -factor yields

$$S_{\text{DC}}(E) = 0.0239 - 0.00693 \cdot E + 0.00257 \cdot E^2 (\text{MeV} \cdot b), \quad (6)$$

for $E_{\text{c.m.}} \leq 1$ MeV.

We have used Eq. (3) to calculate the individual reaction rates for all of the resonances discussed above and for the higher-energy resonances listed in Ref. [17]. An analytic expression for the total reaction rate is

$$\begin{aligned} N_A \langle \sigma v \rangle = & 4.26 \times 10^8 (1 - 0.26T_9 - 0.14T_9^2 + 0.038T_9^3) T_9^{-2/3} \\ & \times \exp(-20.769/T_9^{1/3} - (T_9/0.2)^2) + 85.2 T_9^{-3/2} \\ & \times \exp(-2.793/T_9) + 1.70 \times 10^4 T_9^{-3/2} \\ & \times \exp(-3.428/T_9) + 2.15 \times 10^4 \exp(-5.129/T_9) \\ & + 4.44 \times 10^4 \exp(-6.181/T_9) + [N] 1.39 T_9^{-3/2} \\ & \times \exp(-1.599/T_9) \text{cm}^3 \text{mol}^{-1} \text{s}^{-1}. \end{aligned} \quad (7)$$

The first term describes the contribution from direct capture, while the next two terms represent the dominant low-energy

resonances at 240 and 295 keV. The next two terms are the combined contributions of all higher-energy resonances. The final term is the contribution from the 138-keV resonance, where $N=1$ for s -wave capture. For p -, d -, and f -wave capture, N would be 0.047, 1.7×10^{-3} , and 3.4×10^{-5} , respectively. The total reaction rate and the individual contributions to it are shown in Fig. 8. We also display the rate in tabular form in Table VII. The upper and lower limits listed here include the overall uncertainty of $\pm 40\%$ associated with the direct-capture component along with the combined uncertainties of all important resonances. The latter includes uncertainties in resonance energies and strengths, calculated using the procedures described in Thompson and Iliadis [54]. For all but the lowest temperatures, this corresponds to a 68% confidence belt. Our recommended rate assumes d -wave capture for the 138-keV resonance, which is based on the (unpublished) upper limit for the resonance strength mentioned above. Since this result must be regarded as tentative, it is important to also consider the maximum contribution from this resonance in nucleosynthesis calculations.

2. The $^{23}\text{Na}(p, \alpha)^{20}\text{Ne}$ reaction

An analytic expression for the total (p, α) reaction rate is

$$\begin{aligned} N_A \langle \sigma v \rangle = & 8.06 \times 10^{10} (1 - 4.52T_9 - 265T_9^2 + 7.36 \times 10^3 T_9^3 \\ & - 5.90 \times 10^4 T_9^4 + 1.73 \times 10^5 T_9^5) T_9^{-2/3} \\ & \times \exp(-20.769/T_9^{1/3} - (T_9/0.20)^2) \\ & + 7.98 \times 10^{12} (1 - 46.7T_9 + 960 T_9^2 - 5.90 \\ & \times 10^3 T_9^3 + 1.32 \times 10^4 T_9^4 - 3.83 \times 10^4 T_9^5) T_9^{2/3} \\ & \times \exp(-20.769/T_9^{1/3} - (T_9/0.11)^2) + 3.73 T_9^{-3/2} \\ & \times \exp(-1.967/T_9) + 8.76 T_9^{-3/2} \exp(-2.524/T_9) \\ & + 1.86 \times 10^4 T_9^{-0.195} \exp(-2.981/T_9) \\ & + 3.87 \times 10^6 T_9^{0.751} \exp(-6.019/T_9) \\ & + [0 - 1] 5.35 \times 10^{-15} T_9^{-3/2} \exp(-0.428/T_9) \\ & + [0 - 1] 0.260 T_9^{-3/2} \exp(-1.599/T_9) \text{cm}^3 \text{mol}^{-1} \text{s}^{-1}. \end{aligned} \quad (8)$$

The first two terms describe the respective contributions

TABLE VIII. $^{23}\text{Na}(p, \alpha)^{20}\text{Ne}$ reaction rate.

T_9	Low	Recommended	High
0.010	1.62e-30	2.59e-30	5.49e-30
0.015	2.29e-25	3.67e-25	1.75e-24
0.020	4.07e-22	6.51e-22	1.99e-21
0.025	8.31e-20	1.33e-19	2.62e-19
0.030	4.86e-18	7.78e-18	1.31e-17
0.040	1.87e-15	2.99e-15	4.94e-15
0.050	1.46e-13	2.33e-13	6.71e-13
0.060	5.44e-12	8.46e-12	5.99e-11
0.070	1.68e-10	2.40e-10	2.02e-09
0.080	3.45e-09	4.60e-09	3.00e-08
0.090	4.06e-08	5.22e-08	2.51e-07
0.10	3.01e-07	3.79e-07	1.41e-06
0.11	1.57e-06	1.95e-06	5.86e-06
0.12	6.22e-06	7.51e-06	1.92e-05
0.13	2.13e-05	2.53e-05	5.52e-05
0.14	6.43e-05	7.49e-05	1.41e-04
0.15	1.77e-04	2.02e-04	3.35e-04
0.16	4.53e-04	5.09e-04	7.55e-04
0.18	2.46e-03	2.70e-03	3.44e-03
0.20	1.04e-02	1.14e-02	1.35e-02
0.25	1.63e-01	1.79e-01	1.99e-01
0.30	1.08e+00	1.18e+00	1.30e+00
0.35	4.30e+00	4.66e+00	5.06e+00
0.40	1.28e+01	1.37e+01	1.48e+01
0.45	3.26e+01	3.46e+01	3.67e+01
0.50	7.52e+01	7.93e+01	8.37e+01
0.60	3.17e+02	3.35e+02	3.56e+02
0.70	1.00e+03	1.07e+03	1.14e+03
0.80	2.51e+03	2.68e+03	2.86e+03
0.90	5.26e+03	5.62e+03	6.01e+03
1.0	9.73e+03	1.04e+04	1.12e+04
1.3	3.92e+04	4.15e+04	4.40e+04
1.5	7.84e+04	8.29e+04	8.76e+04
1.8	1.77e+05	1.88e+05	1.97e+05
2.0	2.75e+05	2.90e+05	3.06e+05
2.5	6.25e+05	6.60e+05	6.97e+05
3.0	1.11e+06	1.17e+06	1.23e+06
3.5	1.68e+06	1.78e+06	1.88e+06
4.0	2.30e+06	2.44e+06	2.59e+06
5.0	3.56e+06	3.79e+06	4.05e+06

from subthreshold resonances and the low-energy tails of higher-lying resonances. The next two terms represent the 170- and 217-keV resonances, respectively. The following two terms are the combined contribution from higher-energy resonances. Finally, the two [0–1] terms are the upper limits for the 37- and 138-keV resonances. Since the contribution of the former resonance is small and limited to $T_9 \leq 0.02$, we have ignored it in arriving at a recommended rate. As before, the [0–1] term for the 138-keV resonance assumes s -wave

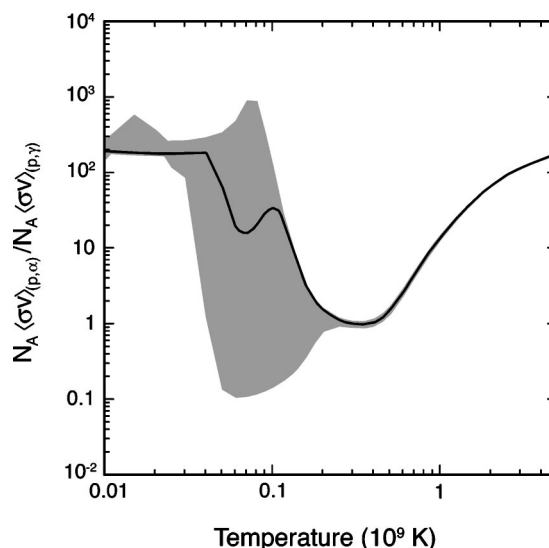


FIG. 10. Ratio of reaction rates for (p, α) and (p, γ) reactions. The solid line is the ratio calculated using the recommended rates and the shaded area denotes the uncertainty in the ratio. The latter includes the correlations in the uncertainties for the two reactions.

capture, whereas for p -, d -, and f -wave capture, the upper limit would be multiplied by 0.047, 1.7×10^{-3} , and 3.4×10^{-5} , respectively. The total reaction rate and the individual contributions to it are shown in Fig. 9. Our recommended rate assumes the upper limit for d -wave capture. The rates listed in Table VIII include the [0–1] terms as well as the 68% confidence belt for the known resonances.

V. CONCLUSIONS

The reaction rates that we have presented here differ quite markedly from those of the NACRE compilation [48] for temperatures below $T_9 \sim 0.2$. For the (p, γ) reaction, the major difference in this work is the inclusion of direct capture, which in fact dominates the rate for $T_9 \leq 0.03$. The uncertain contribution of the 138-keV resonance still causes a large uncertainty for $0.03 \leq T_9 \leq 0.2$. In the case of the (p, α) reaction, we have reduced the maximum contribution of the 37-keV resonance by a factor of 515. Consequently, the uncertainty in this rate is much reduced for $T_9 \leq 0.045$. For example, at $T_9 = 0.03$ the range of uncertainty has been reduced from a factor of 276 to 2.7. The biggest source of uncertainty for the (p, α) reaction is the 138-keV resonance, but it has a much smaller effect in this case than it did for the (p, γ) reaction. For both reactions, the maximum contribution from the 138-keV resonance occurs near $T_9 = 0.07$; here the overall uncertainty is a factor 7.5×10^4 for the (p, γ) reaction and a factor of 12 for the (p, α) reaction.

The competition between (p, γ) and (p, α) determines whether material is trapped within a NeNa cycle or is processed to Mg and Al. Figure 10 shows the ratio of (p, α) to (p, γ) as a function of temperature. Unless the proton width of the 138-keV resonance is near its upper limit, there is strong cycling for $T_9 \leq 0.1$. This has important consequences for the behavior of sodium vs oxygen. To explore

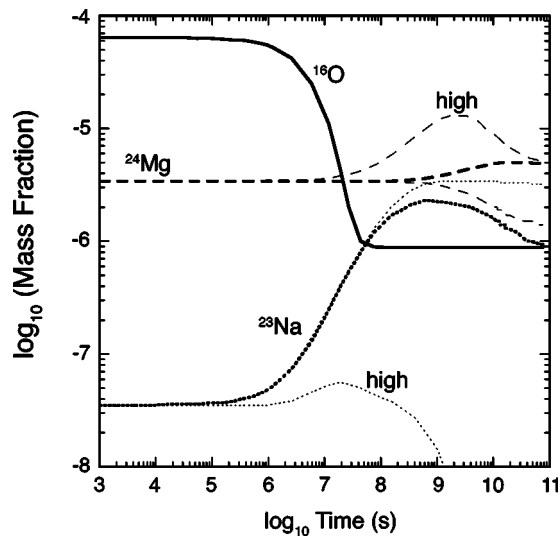


FIG. 11. Network calculation showing the evolution of ^{16}O , ^{23}Na , and ^{24}Mg . The heavy lines are the results using the recommended (p, α) and (p, γ) rates and the lighter lines correspond to the upper (labeled high) and lower (unlabeled) limits.

this effect, we have performed network calculations using the “low,” “recommended” and “high” rates from Tables VII and VIII. The initial abundances were those of an extremely metal-poor star (in this case, a metallicity $Z=0.0002$) with a canonical halo composition (i.e., the alpha elements were enhanced by a factor of 2.5 and ^{23}Na was reduced by the same amount). The temperature and density ($T_9=0.06, \rho$

$=90 \text{ g/cm}^3$) were chosen to be representative of values near the center of the H-burning shell on the red-giant branch. Finally, the calculation was stopped when the hydrogen abundance dropped to 10% of its initial value, which is roughly equivalent to the time required for the H-shell to advance outward by about a shell thickness. The results are shown in Fig. 11. Although there is negligible flow from the CNO nuclei into the NeNa cycle, an apparent Na-O anticorrelation is established if the contribution from the 138-keV resonance is no larger than what is assumed for recommended rates. In this case, the ^{23}Na enhancement relative to iron is well in excess of what is observed, but the maximum Na/O is less. However, this result is not meant to reproduce that of a true model calculation. The important point is that an anticorrelation is not predicted unless the proton width of the 138-keV resonance is near to (or smaller than) the recommended value.

The present uncertainty in the rates of the $^{23}\text{Na}(p, \gamma)^{24}\text{Mg}$ and $^{23}\text{Na}(p, \alpha)^{20}\text{Ne}$ reactions is still large and is dominated by the unknown contributions of the 138-keV resonance. If this state is formed by $\ell \geq 2$ transfer, then its (p, γ) resonance strength could be measured directly. This work is in progress.

ACKNOWLEDGMENTS

We would like to thank P.F. Bertone for his assistance with the experiments described here. This work was supported in part by U.S. DOE Grant No. DE-FG02-97ER41041.

-
- [1] R. P. Kraft, Publ. Astron. Soc. Pac. **106**, 553 (1994).
 - [2] R. P. Kraft, C. Sneden, G. H. Smith, G. E. L. M. Shetrone, and C. A. Pilachowski, Astron. J. **113**, 279 (1997).
 - [3] G. Wallerstein *et al.*, Rev. Mod. Phys. **69**, 995 (1997).
 - [4] C. Sneden, Astrophys. Space Sci. **265**, 145 (1999).
 - [5] P. A. Denisenkov and S. N. Denisenkova, Sov. Astron. Lett. **16**, 275 (1990).
 - [6] R. M. Cavallo, A. V. Sweigart, and R. A. Bell, Publ. Astron. Soc. Pac. **105**, 301 (1993).
 - [7] R. M. Cavallo, A. V. Sweigart, and R. A. Bell, Astrophys. J. **492**, 575 (1998).
 - [8] R. M. Cavallo and N. Nagar, Astron. J. **120**, 1364 (2000).
 - [9] P. A. Denisenkov and A. Weiss, Astrophys. J. **559**, L115 (2001).
 - [10] A. V. Sweigart and J. G. Mengel, Astrophys. J. **229**, 624 (1979).
 - [11] R. C. Gratton, C. Sneden, E. Carretta, and A. Bragaglia, Astron. Astrophys. **354**, 169 (2000).
 - [12] S. E. Hale, A. E. Champagne, C. Iliadis, V. Y. Hansper, D. C. Powell, and J. C. Blackmon, Phys. Rev. C **65**, 015801 (2001).
 - [13] J. Zyskind, M. Rios, and C. Rolfs, Astrophys. J. **243**, L53 (1981); **245**, L97(E) (1981).
 - [14] J. Görres, M. Wiescher, and C. Rolfs, Astrophys. J. **343**, 365 (1989).
 - [15] M. F. E. Eid and A. E. Champagne, Astrophys. J. **451**, 298 (1995).
 - [16] H. Fuchs, K. Grabish, P. Kraatz, and G. Röschert, Nucl. Phys. **A122**, 59 (1968).
 - [17] P. M. Endt, Nucl. Phys. **A521**, 1 (1990).
 - [18] G. Audi and A. H. Wapstra, Nucl. Phys. **A595**, 409 (1995).
 - [19] M. J. S. D. Branford and I. F. Wright, Part. Nuclei **4**, 231 (1972).
 - [20] C. E. Moss, Nucl. Phys. **A269**, 429 (1976).
 - [21] L. K. Fifield, M. J. Hurst, T. J. M. Symons, F. Watt, C. H. Zimmerman, and K. W. Allen, Nucl. Phys. **A309**, 77 (1978).
 - [22] P. Schmalbrock *et al.*, Nucl. Phys. **A398**, 279 (1983).
 - [23] J. D. Garrett, H. T. Fortune, R. Middleton, and W. Scholz, Phys. Rev. C **18**, 2032 (1978).
 - [24] P. D. Kunz, University of Colorado, Boulder, CO, 1978; extended version of J. R. Comfort, 1983.
 - [25] F. D. Becchetti and G. W. Greenless, *Polarization Phenomena in Nuclear Reactions* (University of Wisconsin Press, Madison, 1971).
 - [26] W. W. Daehnick, J. D. Childs, and Z. Vrcelj, Phys. Rev. C **21**, 2253 (1980).
 - [27] C. Iliadis, Nucl. Phys. **A618**, 166 (1997).
 - [28] R. H. Bassel, Phys. Rev. **149**, 791 (1966).
 - [29] P. F. Bertone, A. E. Champagne, M. Boswell, C. Iliadis, S. E. Hale, V. Y. Hansper, and D. C. Powell, Phys. Rev. C **66**, 055804 (2002).

- [30] M. D. Hannam and W. J. Thompson, Nucl. Instrum. Methods Phys. Res. A **431**, 239 (1999).
- [31] S. M. Tang, B. D. Sowerby, and D. M. Sheppard, Nucl. Phys. **A125**, 289 (1969).
- [32] W. J. V. D. M. Pringle and I. F. Wright, Nucl. Phys. **A485**, 380 (1988).
- [33] F. C. Flack, J. G. Rutherglen, and P. J. Grant, Proc. Phys. Soc., London, Sect. A **A67**, 68 (1954).
- [34] T. R. Fisher and W. Whaling, Phys. Rev. **131**, 1723 (1963).
- [35] J. Kuperus, P. W. M. Glaudemans, and P. M. Endt, Physica (Utrecht) **29**, 1281 (1963).
- [36] G. J. Highland and T. T. Thwaites, Nucl. Phys. **A109**, 163 (1968).
- [37] J. R. Vanhoy, E. G. Bilpuch, C. R. Westerfeldt, and G. E. Mitchell, Phys. Rev. C **36**, 920 (1987).
- [38] A. Terakawa *et al.*, Phys. Rev. C **48**, 2775 (1993).
- [39] R. J. Peterson and R. A. Ristinen, Nucl. Phys. **A246**, 402 (1975).
- [40] A. Champagne, P. Magnus, M. Smith, and A. Howard, Nucl. Phys. **A512**, 317 (1990).
- [41] C. Iliadis, L. Buchmann, P. Endt, H. Herndl, and M. Wiescher, Phys. Rev. C **53**, 475 (1996).
- [42] A. Champagne, M. Pitt, P. Zhang, L. Lee, Jr., and M. Levine, Nucl. Phys. **A459**, 239 (1986).
- [43] A. Spadafora and H. T. Fortune, Phys. Rev. C **17**, 1256 (1978).
- [44] J. Vernotte, A. Khendriche, G. BerrierRonsin, S. Grafeuille, J. K. G. Rotbard, R. Tamisier, and B. H. Wildenthal, Phys. Rev. C **41**, 1956 (1990).
- [45] J. Kalifa, J. Vernotte, Y. Deschamps, F. Pougheon, G. Rotbard, M. Vergnes, and B. H. Wildenthal, Phys. Rev. C **17**, 1961 (1978).
- [46] R. L. Kozub and D. H. Youngblood, Phys. Rev. C **5**, 413 (1972).
- [47] D. H. Youngblood, R. L. Kozub, R. A. Kenefick, and J. C. Hiebert, Phys. Rev. C **2**, 477 (1970).
- [48] C. Angulo *et al.*, Nucl. Phys. **A656**, 3 (1999).
- [49] C. M. Rowland, Ph.D. thesis, University of North Carolina at Chapel Hill, 2003.
- [50] B. Paine, S. Kennett, and D. Sargood, Phys. Rev. C **17**, 1550 (1978).
- [51] C. Rowland, C. Iliadis, A. E. Champagne, and J. Mosher, Phys. Rev. C **65**, 064609 (2002).
- [52] J. F. Ziegler and J. P. Biersack, program SRIM2000 (2000), unpublished.
- [53] A. Luukko, A. Anttila, M. Bister, and M. Piiparinen, Phys. Scr. **2**, 159 (1970).
- [54] W. Thompson and C. Iliadis, Nucl. Phys. **A647**, 259 (1999).